Materials Research. 2016; 19(2): 426-433
DOI:http://dx.doi.org/10.1590/1980-5373-MR-2015-0576
© 2016

P(VDF-TrFE)/ZrO_2 Polymer-Composites for X-ray Shielding

Críssia Carem Paiva Fontainha[a], Annibal Theotonio Baptista Neto[b], Adelina Pinheiro Santos[b], Luiz Oliveira de Faria[b]*

[a]Depto. de Engenharia Nuclear, Universidade Federal de Minas Gerais – UFMG, Av. Antônio Carlos, 6627, CEP 31270-970, Belo Horizonte, MG, Brazil
[b]Centro de Desenvolvimento da Tecnologia Nuclear – CDTN, Av. Antônio Carlos 6627, C.P. 941, CEP 31270-901, Belo Horizonte, MG, Brazil

Received: September 25, 2015; Revised: December 14, 2015; Accepted: January 11, 2016

Poly(vinylidene fluoride – tryfluorethylene) [P(VDF-TrFE)] copolymers were mixed with zirconia nanoparticles. The investigation was conducted with the intention to produce nanocompounds with potential to be used as protective patient shielding in radiological procedures. Polymer based nanocomposites with 1, 2, 3, 5 and 10 wt% of ZrO_2 nanoparticles were prepared using sol-gel route with zirconium butoxide as the precursor for zirconium oxide nanoclusters. UV-Vis and FTIR spectrometry and differential scanning calorimetry (DSC) were used to characterize the composite samples. We observed a more homogeneous distribution of ZrO_2 nanoparticles encapsulated by methyl methacrylate (MMA) into the polymeric matrix, when compared to composites made without the use of surface modifiers from methacrylate group. Apparently, this property is related to the absence of the strong MMA absorption band at 1745 cm^{-1}, attributed to C=O bond, in the P(VDF-TrFE)/ZrO_2-MMA nanocomposites. The radiation damage due to high dose exposuring was performed for gamma doses ranging from 100 kGy to 1,000 kGy. The radiation shielding characterization conducted using x-rays with effective energy of 40 keV has demonstrated that composites with 10% of ZrO_2, and only 1.0 mm thick, can attenuate 60% of the x-rays beam.

Keywords: *P(VDF-TrFE)/ZrO_2- MMA polymer composites, ZrO_2 nanoparticles, Radiation protective shielding*

1. INTRODUCTION

Interventional radiology procedures such as fluoroscopy provide high doses to patients because they involve long periods of direct x-rays beam pointing to the same region.[1,2] The procedure is performed in order to guide small instruments such as catheter through blood vessels or other pathways in the body. The tissues near the region of treatment often get exposed to the penetrative X-rays leading to harmful side effects to both internal and superficial organs. Due to the patient scattered radiation, the procedure also contributes to the occupational dose.[3] Nowadays, there is a great interest in developing new radiation attenuator materials that shield part of the incident beam, aiming to minimize the patient skin injuries in specific high dose procedures. However, any attempt to decrease dose in regions of high risk must be always carried out without compromising the fluoroscopic image quality. The design of efficient, lightweight, cost-effective, and flexible materials that provide radiation shielding to patients have drew the attention of several researchers along the world.[4] In this context, composite materials containing compounds or elements with good attenuation properties such as barium sulfate, copper, gadolinium, gold, lead, molybdenum, rhodium, silver, tungsten, bismuth, zirconium oxide, iron oxide and zinc have been studied elsewhere. For instances, bismuth containing composites are today widely applied as protective shielding in radiological CT scans.[5-7]

Polymers are lightweight, conformable, flexible, and easy to process materials. Due to these properties, polymeric based mixtures are ideal candidates to produce thin and lightweight composites required to this application. In this study we report the investigation of polymer nanocomposites filled with zirconium oxide nanoparticles. Poly(vinylidene fluoride-tryfluorethylene) [P(VDF-TrFE)] copolymer is used as the polymeric matrix. In one chemical route, we used non-functionalized zirconia nanoparticles as the filler material. In another route, we used ZrO_2 nanoparticles encapsulated by methyl methacrylate (MMA). This methodology was adopted taking into consideration that the surface modifiers from methacrylate group make the nanoparticles polymerizable in radical polymerization[8] and the existing miscibility between P(VDF-TrFE) copolymers and PMMA.[9] A systematic investigation was conducted in order to evaluate the radiation induced damages and X-rays shielding properties of P(VDF-TrFE)/ZrO_2 nanocomposites with concentrations of 1, 2, 3, 4, 5, 8 and 10 wt% of ZrO_2.

*e-mail: farialo@cdtn.br

2. MATERIALS AND METHODS

Several studies involving composite materials based on a polymer matrix with inorganic nanoparticle report different methods of preparation. Synthesis *in situ* polymerization, sol-gel methods and *in situ* emulsion polymerization have been used to prepare nanocomposites with zirconia as the filler material. In general, polymerization of monomers and the formation of inorganic nanoparticles are made separately. The next step conducts to the formation of nanocomposites by mechanically mixing the polymeric material with the nanoparticles.[10-13] Organic acids have been utilized to improve the compatibility and even to enhance the reactivity of nanoparticles with organic matrix. The surface modifiers from methacrylate group make the nanoparticles polymerizable in radical polymerization.[8] In this context, the use of polymeric materials that form true blends with methacrylic group seems to be the best choice for introducing ZrO_2 nanoparticles in polymeric matrixes. Thus, in view of the reported compatibility between P(VDF-TrFE) copolymers and PMMA, for PMMA contents ranging from 5 to 15 wt%,[9] we also investigated nanocomposites made of P(VDF-TrFE) and ZrO_2 nanoparticles encapsulated with MMA monomers.

The ZrO_2 nanoparticles were prepared according to the route reported by Conceição et al.[14] The sol-gel route uses zirconium butoxide as the precursor for zirconium oxide nanoclusters by controlled hydrolysis and polycondensation. This preparation resulted in the presence of very small aggregates, with average diameters around 100 nm. The functionalized zirconia nanoparticles were obtained *in situ* by introducing methacrylic acid as an organic modifier group.

Poly(vinylidene fluoride – trifluorethylene) copolymers [$P(VDF\text{-}TrFE)_{50/50}$] were dissolved in DMAc (*n,n*-dimethylacetamide). Two batches were produced: one with pure ZrO_2 nanoparticles (P(VDF-TrFE)/ZrO_2 nanocomposite) and another with MMA surface-modified ZrO_2 nanoparticles), both added to the solution with concentrations of 1, 2, 3, 4, 5, 8 and 10 wt% of ZrO_2. Films with c.a. 70μm were obtained after complete solvent evaporation at 60 °C. For comparison purposes, we have also produced a batch of P(VDF-TrFE)/PMMA blends with different contents of PMMA by dissolving the components in DMAc with subsequent evaporation at 60 °C. The composites characterization has been made by UV-Vis and Fourier-transform Infrared spectroscopy (FTIR) and differential scanning calorimetry (DSC). Optical absorption measurements were taken in a Shimadzu UV-240 PC spectrometer at wavelengths ranging from 190 to 900 nm. The FTIR spectra were measured at a BOMEM 100 spectrometer for wavenumbers ranging from 200 to 4,000 cm^{-1}. The FTIR measurements were performed using Transmission mode by putting the films directly exposed to the FTIR beam. The beam was always focused in the center of each c.a. 70μm film sample. By using this methodology we assume that the quantities of ZrO2 were in principle homogeneously distributed inside the polymeric matrix. Thermal behavior studies were made using a DSC TA Q10, with heating and cooling rates of 10 °C/min, in the second run, from 25 to 180 °C.

Radiation shielding characterization was performed by sandwiching P(VDF-TrFE)/ZrO_2 films between two external layers both containing two thermoluminescent dosimeters (TLD) each. In this setup, one layer is directly exposed to the x-rays beam and the other measures the attenuated beam. We have used the commercially available thermoluminescent dosimeters LiF:Mg,Ti (TLD-100). TL output measurements were taken using a Harshaw-Bicron 4500 reader, with heating rate of 10°C/s. All TLD-100 dosimeters were previously irradiated at the same dose (10 mGy) for the beam qualities RQR2 (40kV) and RQR5 (70kV) and their TL output were used to obtain an individual correction factor for each chip belonging to the calibration batch. The radiation induced damages were evaluated using high gamma dose irradiation, performed in a Co-60 source at constant dose rate (12 kGy/h), with doses ranging from 100 to 1,000 kGy.

3. RESULTS AND DISCUSSION

3.1 Composite Characterization

In the visual analyses of the two batches produced, we have found discrepant differences between the distributions of ZrO_2 nanoparticles into the P(VDF-TrFE) host matrix. In samples produced without MMA, it was possible to see, with naked eye, some clusters while samples produced with MMA show no visible clusters. In Fig. 1, we show the SEM images for samples of P(VDF-TrFE)/ZrO_2 nanocomposites with 2.0 wt% of pure ZrO_2 nanoparticles, prepared without MMA (left) and samples prepared with functionalized zirconia nanoparticles (right). The clusters seen in the left side (sample without MMA, scale 1μm) were identified as ZrO_2 nanoparticles. Note that in the SEM image at right (sample with MMA, scale 200 nm) there are no clusters, with a homogeneous distribution of ZrO_2 nanoparticles. Based on the above observations, in this work we will report results only for this methodology. We note that, apparently, the compatibility between P(VDF-TrFE) copolymers and MMA monomers favours a more homogenous distribution of MMA monomers into the P(VDF-TrFE) host matrix and, consequently, a more homogeneous distribution of ZrO_2 nanoparticles. We remark that PMMA and P(VDF-TrFE) form true blends only for increasing PMMA contents ranging from 5 to 15 wt%. Above this value, the components are not mixed. This behavior was observed by measuring the glass transition temperature (T_G) of the blend, which in turn must follow the classic Gordon-Taylor curve for compatible polymer blends.[9,15] Then, although we have produced no samples with ZrO_2 contents above 10 wt%, it is expected that the homogeneous distribution of encapsulated ZrO_2 nanoparticles observed in Figure 1 (upper) may not be the same for ZrO2 contents higher than 15 wt%.

In order to investigate the optical changes induced by the addition of ZrO_2-MMA nanoparticles into the P(VDF-TrFE) matrix, we have collected the UV-Vis spectra for all ZrO_2 compositions in the ultraviolet-visible spectral range. They are shown in Fig. 2(a). In Fig. 2(b), for comparison purposes, we show the spectra for pristine P(VDF-TrFE), P(VDF-TrFE)/PMMA blend with 5 wt% of PMMA and P(VDF-TrFE)/ZrO_2-MMA nanocomposite with 5 wt% of ZrO_2-MMA. Looking at the spectra of Fig. 1(a) we see that there is a gradual increasing in the absorbance intensities in the 200-350 nm range for increased amounts of ZrO_2 in the composite. These overlapped absorption bands are attributed

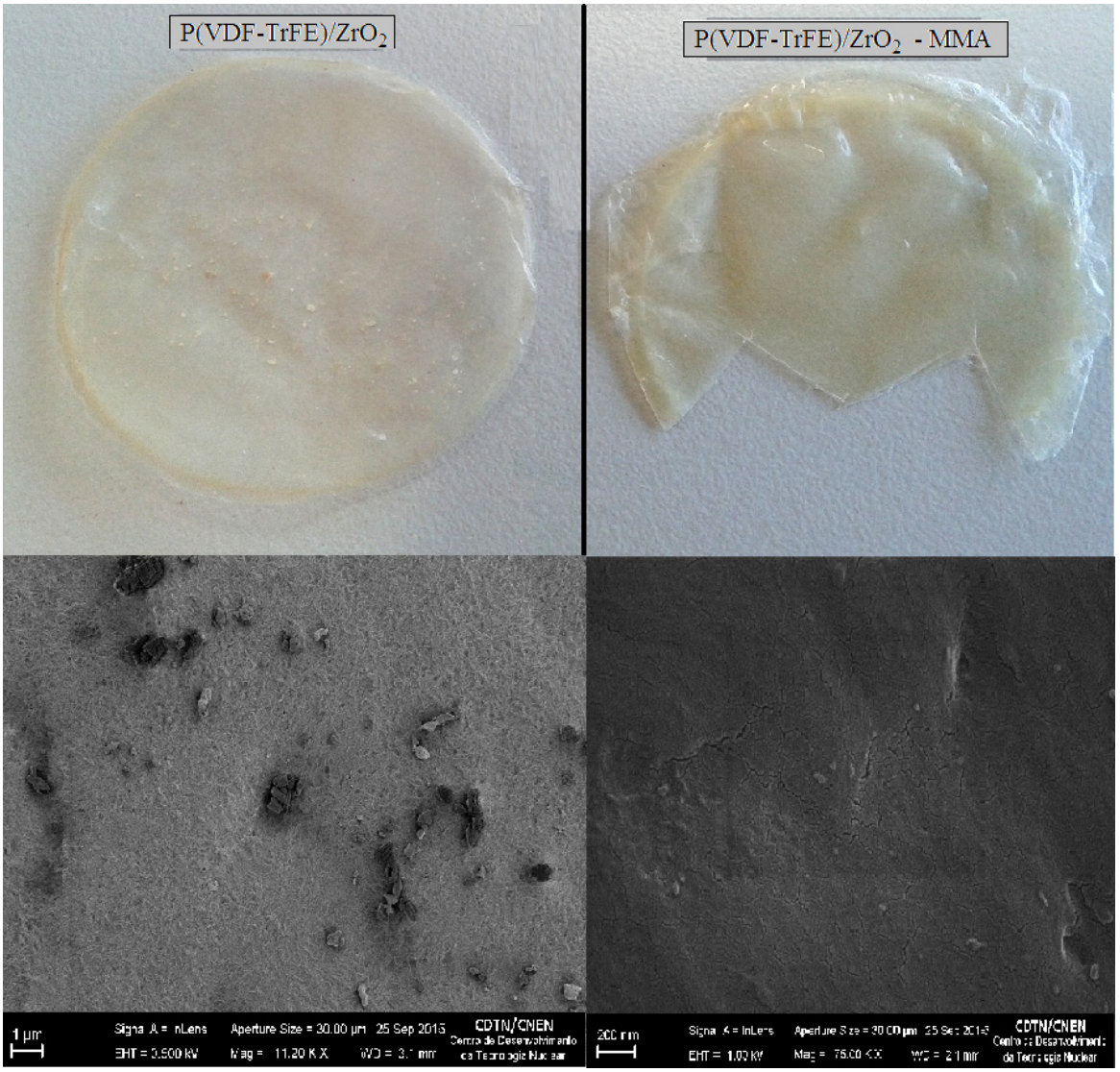

Fig. 1 – Photographs (upper) and SEM images taken on the surface of P(VDF-TrFE)/ZrO_2 nanocomposites samples with 2.0 wt% of pure ZrO_2 (bottom), prepared without MMA (left) and samples prepared with 2% of functionalized zirconia nanoparticles(right).

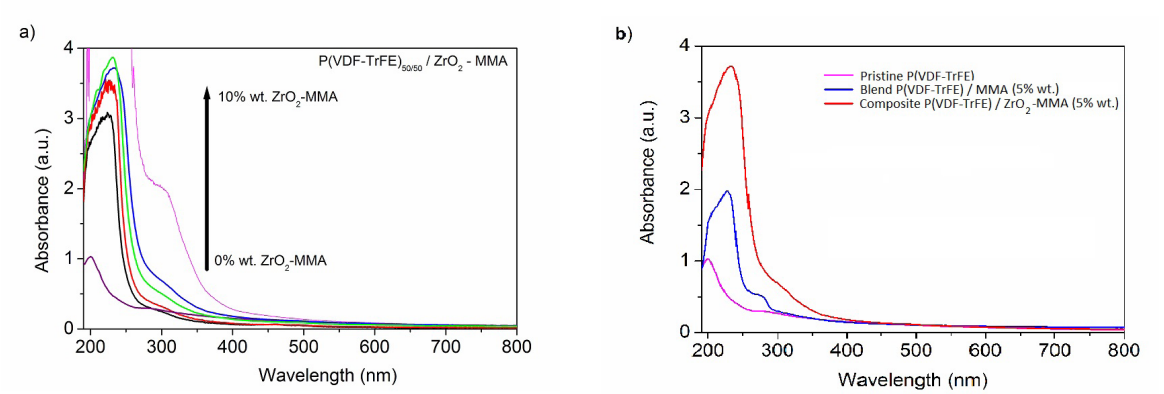

Fig. 2 – UV-Vis absorbance spectra for (a) P(VDF-TrFE)/ZrO_2-MMA nanocomposites doped with 1, 2, 3, 5 and 10 wt% of functionalized ZrO_2 nanopartcles and (b) pristine P(VDF-TrFE), P(VDF-TrFE)/PMMA blend with 5 wt% of PMMA and the P(VDF-TrFE)/ZrO_2-MMA nanocomposites with 5 wt% of ZrO_2.

to the sum of the p - p* transitions of PMMA absorption band, which starts around 270nm and attains its maximum at 226 nm, and the ZrO_2 absorption band, which starts around 400 nm and attains its maximum at 270 nm, as one can be inferred from Fig 2(b). These UV absorption bands have also been observed by Hu et al.,[16] in a very interesting work about properties of transparent PMMA/ZrO_2 composites, with 0.8, 5 and 7 wt% of ZrO_2, made by *in-situ* polymerization of MMA/ZrO_2 dispersion. Actually, as it was not possible to produce pure MMA/ZrO_2 composites in our work, because of the methodology used, we have attributed the absorption band at 270 nm to ZrO_2 based on information provided in that reference. The overall absorbance observed for wavelengths ranging from 400nm to 800 nm in Fig. 1(a) indicates that the nacomposites are totally transparent in this visible spectral region. We remark that transparent protective garments can be very useful during interventional procedures in order to control the damage levels to patient skin provoked by the incident X-rays.

We may now investigate if the reported miscibility between P(VDF-TrFE) copolymers and PMMA, for 5, 10, 15 and 30 wt% of PMMA contents[9] could be somehow taking place in P(VDF-TrFE)/ZrO_2–MMA nanocomposites, providing a more homogeneous distribution of ZrO_2 nanoparticles into the polymer matrix. Thus, in Figure 3 we show the FTIR transmission spectra for P(VDF-TrFE)/ZrO_2–MMA composites with 0, 1, 2, 3 and 5 at.% of ZrO_2 and also for pristine P(VDF-TrFE) sample, for spectral regions ranging from (a) 300 to 1050 cm^{-1} and (b) and from 1300 to 1850 cm^{-1}. Figures 3(c) and 3(d) compare the FTIR spectra for c) pristine P(VDF-TrFE) copolymers and P(VDF-TrFE)/ZrO_2-MMA composites with 1 wt% of ZrO_2 and d) pure MMA, for wavenumbers ranging from 500 to 3800 cm^{-1}. The FTIR spectrum for the sample with 10 wt% of ZrO_2 is not shown here in view of the saturation of the transmission intensities in several spectral ranges studied. In Fig. 3(a) we can see the gradual increase of the absorbance intensities at 466, 591, 660 and 945 cm^{-1}, for increasing amounts of ZrO_2-MMA in the composite. The absorptions at 466 and 591 cm^{-1} are attributed to the stretching of Zr-O bonds in ZrO_2 whereas the absorptions at 660 and 945 cm^{-1} are related to the bending of O-C=O and =CH out-of-plane deformation in MMA, respectively.

For clarity purposes we plot in Fig. 3(b) a zoom for wavenumbers ranging 1300 to 1850 cm^{-1}, in view of the following observations. There is a gradual increase of the absorption intensities at 1450, 1555, 1645 and 1700 cm^{-1} for increasing amounts of ZrO_2-MMA in the composite. The band at 1450 cm^{-1} is attributed to sum of the scissors vibration of CH_2 and the antisymetric deformation of CH_3 molecules in MMA.[16] The high absorption seen at 1555 cm^{-1} is attributed to the stretching of Zr-O bonds whereas the bands at 1645 and 1705 cm^{-1} may be attributed to the stretch of C=O bonds in MMA.

In view of some reported evidences concerning the absorption band at 1645 cm^{-1}, we may discuss it in more detail. We remark that Faria and Moreira [17] have observed an absorption band at 1643cm^{-1} in P(VDF-TrFE)/PMMA blends which is active only for the mixtures. This absorption band is clearly an experimental evidence of the strong

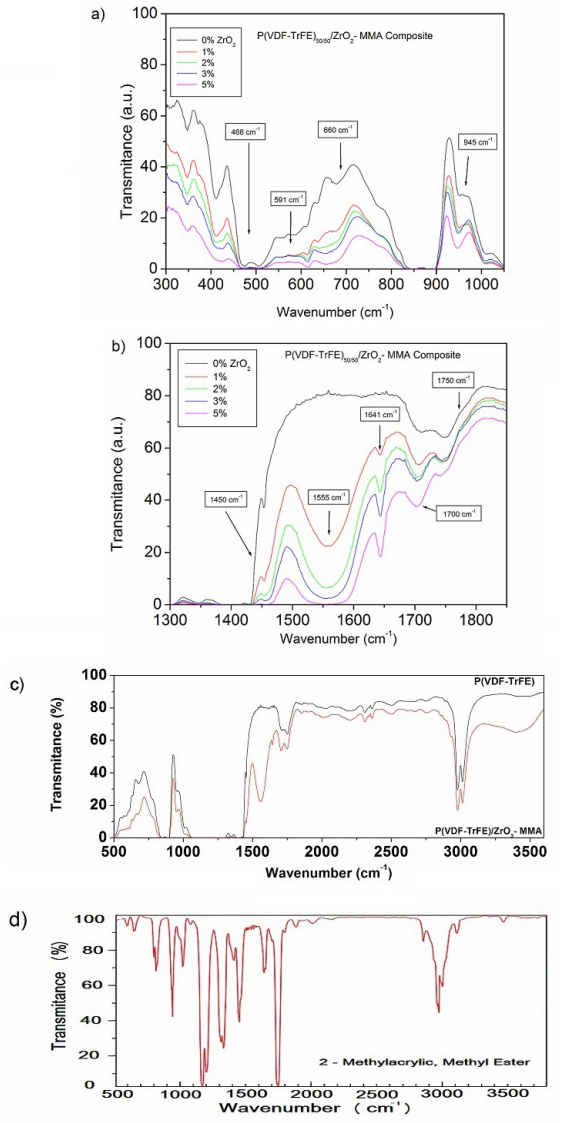

Fig. 3 - FTIR spectra for P(VDF-TrFE)/ZrO_2-MMA nanocomposites films with 0, 1, 2, 3 and 5 wt% of ZrO_2 for a) wavenumbers ranging from 300 to 1050 cm^{-1} and b) the spectral region between 1300 to 1850 cm^{-1}. Figures 3(c) and 3(d) compare the FTIR spectra for c) pristine P(VDF-TrFE) copolymers and P(VDF-TrFE)/ZrO_2-MMA composites with 1 wt% of ZrO_2 and d) pure MMA, for wavenumbers ranging from 500 to 3800 cm^{-1}.

interaction between the copolymer and the PMMA chains. Thus, we think that this could be an alternative explanation for the band at 1645 cm^{-1}. On the other hand, we see that the strong MMA absorption band at 1740 cm^{-1} in Fig. 3(d), also attributed to C=O bond, is absent in the nanocomposites spectra of Fig. 3(b), for all ZrO_2 compositions. However, this intense absorbance band is reported to be present in the PMMA/ZrO_2 nanocomposites made by different methods, for all ZrO_2 concentrations studied.[10,13,16] It is also present in P(VDF-TrFE)/PMMA blends, for all PMMA contents, but downshifted to 1735 cm^{-1}. [17] Although a conclusive explanation to this phenomenon requires additional investigations and calculation by molecular modeling, we suggest that the

absorption band at 1645 cm^{-1} could be originated by the weakening of the C=O bond, which could also be sharing its electronic charge with the P(VDF-TrFE) copolymer chain, decreasing its intensity at 1745 cm^{-1}. In this mechanism, the hydrogen from the copolymer chain interacts with carbonyl from the ZrO_2-MMA nanoparticles. In this respect, we note that Coleman et al., [18] suggested that the carbonyl group could be involved in the interaction between PMMA and PVDF in binary blends of these two constituents. The interaction between the P(VDF-TrFE) copolymer chain and the carbonyl group could explain the observed better homogeneous distribution of ZrO_2 nanoparticles into the polymeric matrix, when compared to composites made without the use of surface modifiers from methacrylate group.

In the far IR spectral region shown in Fig. 3(c) we see again the gradual increase of the absorption intensities at 2850, 2970, 3110 and 3428 cm^{-1} for increasing amounts of ZrO_2-MMA in the composite. The absorption bands at 2850 and 2970 are attributed to the CH stretching modes in O-CH_3 bonds and to the antisymetric and symmetric stretching in CH_2 and CH_3 bonds, respectively. On the other hand, we see that the weak absorption band at 3110 cm^{-1} and the large one at 3428 cm^{-1} could be only attributed to O-H stretching bonds. In fact, in the preparation of our samples with ZrO_2-MMA there was addition of water in the mixture suspension.[14] Also, in this respect, we note that the FTIR data collected at higher temperatures for PMMA/ZrO_2 nanocomposites reported in the literature have clearly demonstrated the absence of these absorption bands above 100°C.[10,16]

DSC thermograms were collected in order to detect changes in the $P(VDF\text{-}TrFE)_{50/50}$ crystalline structure provoked by the addition of ZrO_2-MMA nanoparticles. This DSC data could be of great help in view of well known ferroelectric behavior of P(VDF-TrFE) that presents a ferroelectric-to-paelectric (f-p) phase transition for trifluorethylene contents ranging from 18 to 63 mol%.[19] Similarly to ferromagnetic materials, the temperature of the F-P transition is called the Curie Temperature (T_C). The P(VDF-TrFE) with 50 wt% of TrFE monomers used in this work is particularly important because its T_C occurs around 65°C, far below the melting temperature (T_M) that occurs around 160°C. This behavior allows us to simultaneously observe two kind of phase transition during the same scan. We remark that both phase transitions give information about the crystalline structure. The F-P transition is related to the chain configuration inside the crystalline lamellae and the melting transition is related to the crystalline-amorphous transition. In Fig. 4 we show the differential scanning calorimetry (DSC) thermograms for P(VDF-TrFE/ZrO_2-MMA nanocomposites with different concentrations (0, 1, 5 and 10 wt%) of ZrO_2. For pristine P(VDF-TrFE) copolymers, on the heating cycle, we see two diffuse endothermic peaks centered at 63.2°C and 160.2 ºC, respectively. The low temperature peak is attributed to the well-known ferroelectric-to-paraelectric phase transition of pristine P(VDF-TrFE) copolymer.[20] The higher temperature peak is attributed to the melting phase transition of the P(VDF-TrFE) crystalline portion. Comparing the DSC curves of pristine P(VDF-TrFE) and the P(VDF-TrFE)/ZrO_2–MMA nanocomposites with 1 wt% of ZrO_2, we see a decrease in the melting temperature (T_M), from 160.2ºC to 155.3°C,

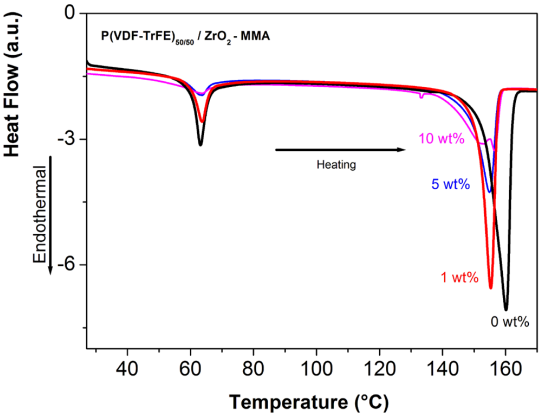

Fig. 4 - DSC thermograms of P(VDF-TrFE)/ZrO_2 nanocomposites films with concentrations of 0, 1, 5 and 10 wt% of ZrO_2 nanoparticles.

respectively, while almost no change is observed for T_C, which changes from 63.2 to 63.3°C. The evaluated melting latent heat (L_M), which can be inferred from the area under the endothermic peaks, decreases from 28.0 to 26.4 J/g. However, when we increase the ZrO_2 content from 1 to 5 wt% of ZrO_2, the melting temperature is little affected while the melting latent heat (crystalline volume) decreases from 26.4 to 15.4 J/g. In summary, we can say that T_C is kept constant for all compositions while T_M decreases around 5°C from 0 to 1 wt%, remaining constant for all other compositions. On the other hand both melting latent heat and F-P latent heat transition continuously decrease for increased amounts of ZrO_2, indicating that there is a continuous decrease in the crystalline volume of the nanocomposites. The initial decrease of T_M (~5°C) for samples with 0 wt% to 1 wt% of ZrO_2 tell us that P(VDF-TrFE) crystalline order is initially decreased, keeping constant for higher contents. The reducing of the F-P latent heat transition also denotes a gradual loss of stability of the ferroelectric phase.We remark that the constancy of T_C for increasing ZrO_2 contents means that the electric dipolar orientation along the crystallites, i.e. from one crystallite to the neighbours crystallites, is not affected, at least for the concentrations studied. In other words, it means that there is a weak interaction between the ZrO_2-MMA nanoparticles and the copolymer chains in the amorphous phase, allowing the establishment of long-range ferroelectric order among the crystallites.

3.2 Radiation Shielding and Damage Characterization

In this section we will evaluate the shielding properties and radio-induced damages of P(VDF-TrFE)/ZrO_2-MMA nanocomposites exposed to high energy radiation fields. As we intend to develop new radiation attenuator materials that shield part of the incident beam in specific high dose interventional procedures, we will evaluate the radiation attenuation coefficients for x-rays of a RQR2 beam quality, whose photons have an Effective Energy (E_{eff}) around 40 keV. The calibration curve obtained for these conditions is $D = L/a$ where D is the radiation dose (mGy), L is the electric charge

in the photomultiplier tube (nC) and *a* is the conversion factor obtained during the previous calibration equal to 47.77 nC.mGy^{-1}. After irradiating samples with 1, 2, 3, 5 and 10 wt% we have found an increasing attenuation for increased amounts of ZrO_2. The sample with 10 at. % has provided an attenuation of 6.5% in the X-rays beam, for films only 70µm thick. In order to compare the shielding properties of the nanocomposites studied with the shielding properties of pure ZrO_2 we have estimated their mass attenuation coefficient and also their density. The mass attenuation coefficient can be inferred from the known expression

$$I / I_0 = e^{-(M/P).PX} \quad (1)$$

where I and I_0 are the attenuated and initial intensities, respectively, (μ/ρ) is the mass attenuation coefficient in cm^2/g, ρ is the material density in g/cm^3 and x is the film thickness in cm. In Fig. 5 we plot the attenuation curves for pure ZrO_2, P(VDF-TrFE)/ZrO_2 nanocomposites with 5.0 and 10.0 wt% ZrO_2 and PMMA, as a function of thickness. We have plotted the curve for PMMA because it has almost the same density as P(VDF-TrFE), just for comparison purposes. We remark that for nanocomposites with 10% of ZrO2 and only 1.0 mm thick, the beam attenuation is higher than 0.6, with a density of only 2.20 g/cm^3.

We may now discuss about the estimation of the radio-induced damages of these polymer nanocomposites provoked by successive exposures to ionizing radiation beams. This issue is directly linked to the economic practical aspects involved in the life cycle of shielding protective clothes, once the defects induced by ionizing radiation in macromolecules are known to be cumulative for continuous exposuring. It is well known that for most interventional radiology procedures elsewhere, there is little or no information on skin dose, either for average dose or for the frequency with which skin dose exceed a given threshold.[21] However, a comprehensive study made by Balter et al., [22] revealed that, depending on the kilo-voltage applied and also on the equipment used, these doses can vary from 6 to 60 mGy for each acquisition. In this work we will use FTIR spectrometry aiming the analysis of the extinction and production of new chemical bonds provoked by radiation exposure.

In order to estimate the radio-induced damages in the P(VDF-TrFE)/ZrO_2–MMA nanocomposites we started the investigation exposing this material to high doses of gamma radiation. In this context we have exposed pristine P(VDF-TrFE) copolymers and P(VDF-TrFE)/ZrO_2-MMA nanocomposites with 5 wt% of ZrO2 to 100, 500 and 1,000 kGy to a radiation field, using a ^{60}Co gamma source. In this respect, we note that once the radiation dose is expressed in "kGy" units, the radiation quality factor used elsewhere to estimate the damages to any target material is equal to 1.0 for both X-rays (E_{eff} = 40 keV) and gamma rays (E = 1250 keV), in spite of the difference in their photon energies. The FTIR spectra collected just after the irradiation process are shown in Fig. 6, for wavenumbers ranging from 1500 to 2000 cm^{-1}. Although some changes in the absorption bands have also been observed in the 2500-3600 cm^{-1} and 400-700 cm^{-1} region, we picked out this region for clarity purposes. It is seen in Fig. 6(a) that the stretching ZrO_2 absorption band at 1555 cm^{-1} strongly decreases its intensity for increasing gamma doses, as well as the band at 1645 cm^{-1} attributed to the stretch of C=O bonds in MMA. We remind that the absorption band at 1645 cm^{-1}, as discussed in the characterization section, could be also originated by the weakening of the C=O bond at 1745cm^{-1}, which in turn would be sharing its electronic charge with the P(VDF-TrFE) copolymer chain by the formation of hydrogen bonds. As a matter of fact, all absorption bands attributed to ZrO_2 and MMA seen in Fig. 2(a) and 2(b) have their intensities decreased for increasing radiation doses. Further investigation is now in progress in order to find out the behaviour of the shielding properties after the radiation induced decrease of the ZrO_2 and MMA attributed bands. On the other hand, it is also possible to see, in Fig. 6, the increase of the absorption band at 1729 cm^{-1}, for increasing doses. This band is elsewhere attributed to the formation of C=O bonds and corresponds to the C=O dimmer stretch in CF2–CH2–COOH chemical ligation that is formed after the rupture of the $[CH_2\text{-}CF_2]_n$ monomers in

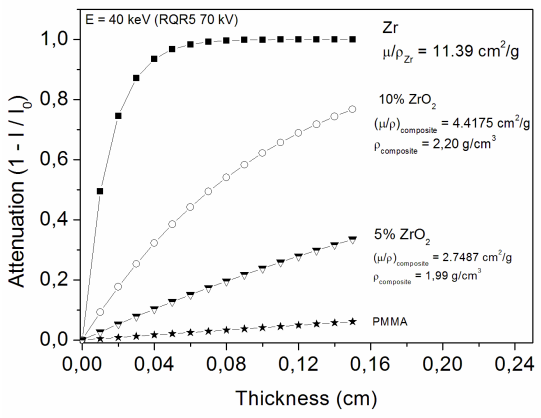

Fig. 5 Plot of the *Attenuation x Thickness* curve for pure ZrO_2, P(VDF-TrFE)/ZrO_2 composites with 5.0 and 10,0 at.% ZrO_2 and PMMA. For pure ZrO_2 and PMMA we have used the mass attenuation coefficient provided by NIST institute.

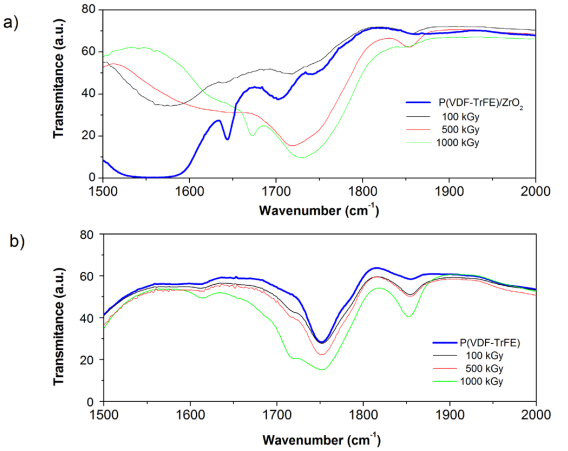

Fig. 6 – FTIR transmittance spectra of a) P(VDF-TrFE)/ZrO_2–MMA nanocomposites with 5 wt% of ZrO_2 and b) pristine P(VDF-TrFE), exposed to 0, 100, 500 and 1,000 kGy of gamma radiation.

Table 1 – FTIR absorbance intensities for absorptions peaks at 591, 660, 1450, 155, 1641, 1672, 1729 and 1853cm^{-1} for pristine P(VDF-TrFE)/ZrO_2–MMA nanocomposites and irradiated with 100, 500 and 1,000 kGy of gamma photons.

	Pristine Abs (a.u)	100 kGy Abs (a.u)	500 kGy Abs (a.u)	1000 kGy Abs (a.u)	Attribution
591 cm^{-1}	2.18	0.98	0.97	0.98	Stretching Zr-O in ZrO_2
660 cm^{-1}	1.83	0.62	0.61	0.59	bending of O-C=O in MMA
1450 cm^{-1}	2.93	0.59	0.57	0.56	vibration of CH_2 in MMA
1555 cm^{-1}	2.68	0.47	0.35	0.21	Stretching ZrO_2
1641 cm^{-1}	0.72	0.38	0.50	0.44	C=C stretch in MMA-modified ZrO_2 nanoparticles
1672 cm^{-1}	0.36	0.29	0.51	0.68	C=O stretch or C=C stretch
1729 cm^{-1}	0.30	0.31	0.75	1.01	C=O dimer stretch in CF2–CH2–COOH
1853 cm^{-1}	0.16	0.16	0.20	0.20	C=O stretch in CF2-CH2-COF

PVDF homopolymer or P(VDF-TrFE) and P(VDF-HFP) copolymers chain scission.[23] For practical purposes we show in Table 1 the behaviour of the absorption bands at 591, 660, 1450, 1555, 1641, 1672, 1729 and 1853 cm^{-1} after the irradiation process. Finally, we observe that the absorption peak at 1672 cm^{-1} starts to be prominent only for gamma doses above 500 kGy. It is well shaped for 1000 kGy in P(VDF-TrFE)/ZrO_2-MMA composites but it is not so well defined in pure P(VDF-TrFE) copolymers. This observation lead us to believe that absorption band at 1672 cm^{-1} may be linked to the radio-induction of C=O or C=C bonds in the MMA monomers. We remark that the amount of ZrO_2 nanoparticles encapsulated by MMA present in these samples is only 5 wt%, which would explain the appearance of a well defined peak only for higher gamma doses.

On the other hand, recently, a systematic study about the influence of lower doses of ionizing radiation on the P(VDF-TrFE) crystalline structures revealed that there were no significant changes in the crystalline parameters, i. e. T_C, T_M, L_C and L_M, measured by DSC, for doses ranging from 0.3 to 1.0 kGy.[24] In another report, the FTIR and UV-Vis data also suggests that gamma radiation provokes barely destruction of the existing polymeric chemical bonds and the creation of small amounts of C=C and C=O bonds, respectively.[25] Based on these data, we have estimated that P(VDF-TrFE)/ZrO_2-MMA composites could probably be used as protective shielding for at least 16,000 image acquisitions.

CONCLUSIONS

Polymer nanocomposites made of P(VDF-TrFE) copolymers mixed with different amounts of surface-modified ZrO_2 nanoparticles were prepared and characterized. We observed a more homogeneous distribution of ZrO_2 nanoparticles into the polymeric matrix, when compared to composites made without the use of surface modifiers from methacrylate group. UV-Vis spectroscopic data indicates that the P(VDF-TrFE)/ZrO_2-MMA nanocomposites are highly transparent in the 400-800nm visible spectral region. FTIR spectroscopy studies revealed that the strong absorption band at 1745 cm^{-1}, attributed to C=O bonds of MMA, is not present in the P(VDF-TrFE)/ZrO_2-MMA nanocomposites. DSC data evinced a gradual decrease in the crystalline volume of the polymer composites for increased ZrO_2 contents. In the radiation damage analysis, FTIR data revealed that absorption bands attributed to ZrO_2 bonds and MMA C=O bonds are strongly reduced for gamma doses ranging from 100 to 1,000 kGy. Radiation shielding characterization demonstrates that composites with 10% of ZrO_2, and only 1.0 mm thick, can attenuate 60% of the x-rays beam. These results indicate that P(VDF-TrFE)/ZrO_2-MMA polymer composites are good candidates to be explored as light-weighted and flexible protective shielding for application in radiological procedures.

Acknowledgements

This work was supported by Conselho Nacional de Desenvolvimento Científico e Tecnológico (CNPq), Fundação de Amparo à Pesquisa do Estado de Minas Gerais (FAPEMIG) and Comissão Nacional de Energia Nuclear (CNEN).

References

1 - Miller DL, Balter S, Cole EP, Lu TH, Schueler BA, Geisinger M, Berenstein A, Albert R, Georgia JG, Noonan PT, Cardella JF, George JS, Russell EJ, Malisch TW, Vogelzang RL, Miller III GL, Anderson J; RAD-IR Study. Radiation doses in interventional radiology procedures: The RAD-IR study part I: Overall measures of dose. *Journal of Vascular Interventional Radiology.* 2003;14(6):711–727.

2 - Brambilla M, Marano G, Dominietto M, Cotroneo AR, Carriero A. Patient radiation doses and references levels in interventional radiology. *La Radiologia Medica.* 2004;107(4):408-418.

3 - Trianni A, Chizzola G, Toh HE, Quai E, Cragnolini G, Bernardi A, et al. Patient skin dosimetry in haemodynamic

and electrophysiology interventional cardiology. *Radiation Protection Dosimetry*. 2005;117(1-3):241-246.

4 – Nambiar S, Yeow JT. Polymer-composite materials for radiation protection. *ACS Applied Materials & Interfaces*. 2012;4(11):5717−5726.

5 - McCaffrey JP, Downton B, Shen H, Mainegra-Hing E. Radiation attenuation by lead and nonlead materials used in radiation shielding garments. *Medical Physics*. 2007;34(2):530-537.

6 - Parker MS, Chung JK, Fatouros PP, Hoots JA, Kelleher NM, Benedict, SH. Reduction of radiation dose to the female breast: preliminary trails with a custom designed tungsten-antimony composite breast shield. *The Journal of Applied Research*. 2006;6(3):230-239.

7 - Iball GR, Kennedy EV, Brettle DS. Modelling the effect of lead and other materials for shielding of the fetus in CT pulmonary angiography. *The British Journal of Radiology*. 2008; 81(966):499-503.

8 - Xu K, Zhou S, Wu L. Dispersion of γ-methacryloxypropyltrimet hoxysilane-functionalized zirconia nanoparticles in UV-curable formulations and properties of their cured coatings. *Progress in Organic Coatings*. 2010;67:302-310.

9 - Faria LO, Moreira RL. Structural and kinetic transitions In P(VDF-TrFE)/PMMA blends. *Polymer*. 1999;40(16):4465-4471.

10 - Motaung TE, Luyt AS, Saladino ML, Martino DC, Caponetti E. Morphology, mechanical properties and thermal degradation kinetics of PMMA-zirconia nanocomposites prepared by melt compounding. *Express Polymer Letters*. 2012;6(11):871-881.

11 - Duan G, Zhang C, Li A, Yang X, Lu L, Wang X. Preparation and characterization of mesoporous zirconia made by using a poly (methyl methacrylate) template. *Nanoscale Research Letters*. 2008;3(3):118-122. doi: 10.1007/s11671-008-9123-7

12 - Hu Y, Zhou S, Wu L. Surface mechanical properties of transparent poly(methyl methacrylate)/zirconia nanocomposites prepared by *in situ* bulk polymerization. *Polymer*. 2009;50(15):3609-3616. DOI: 10.1016/j.polymer.2009.03.028

13 - Haldorai Y, Zong T, Shim J. Core-shell ZrO_2/PMMA composites via dispersion polymerization in supercritical fluid: Synthesis, characterization and mechanism. *Journal of Applied Polymer Science*. 2012;123(2):1176-1183. DOI: 10.1002/app.34688

14 - Conceição PV, Faria LO, Santos AP, Furtado CA. Study of bare functionalized zirconia nanoparticles filled polymer electrolytes based on a polyurethane. *MRS Symposium Proceedings*. 2003;756:EE3.14.1-14.6.

15 - Roerdink E, Challa G. Influence of tacticity of poly(methyl methacrylate) on the compatibility with poly(vinylidene fluoride). *Polymer*. 1978;19(2):173-178. DOI: 10.1016/0032-3861(78)90034-4

16 - Hu Y, Gu G, Zhou S, Wu L. Preparation and properties of transparent poly(methyl methacrylate)/zirconia nanocomposites using 2-hydroxyethyl methacrylate as a coupling agent. *Polymer*. 2011;52(1):122-129. DOI: 10.1016/j.polymer.2010.11.020

17 - Faria LO, Moreira RL. Infrared spectroscopic investigation of chain conformations and interactions in P(VDF-TrFE)/PMMA blends. *Journal of Polymer Science: Part B*. 2000;38(1): 34-40.

18 - Coleman MM, Zarian J, Varnell DF, Painter PC. A fourier transform infrared study of polymer blends. I. Poly(vinylidene fluoride) — poly(methyl methacrylate) system. *Journal of Polymer Science: Polym Letters Edition*. 1977;15(12):745-750. DOI: 10.1002/pol.1977.130151207

19 - Lovinger AJ. Ferroelectric polymers. *Science*. 1983;220(4602):1115-1121.

20 – Moreira RL, Lobo RP, Medeiros-Ribeiro G, Rodrigues WN. The diffuse behavior of the ferroelectric transition in poly(vinylidene fluoride-trifluoroethylene) copolymers. *Journal of Polymer Science Part B*. 1994;32(5):953-959. DOI: 10.1002/polb.1994.090320518

21 - Johnson DR, Kyriou J, Morton EJ, Clifton A, Fitzgerald M, Macsweeney E. Radiation protection in interventional radiology. *Clinical Radiology*. 2001;56(2):99-106.

22 - Balter S, Schueler BA, Miller DL, Cole PE, Lu HT, Berenstein A, et al. Radiation doses in interventional radiology procedures: The RAD-IR Study: Part III: dosimetric performance of the interventional fluoroscopy Units. *Journal of Vascular and Interventional Radiology*. 2004;15(9):919-916.

23 - Boullier I, Esnouf S, Le Moël A. Radiooxidation of fluoropolymers: identification of oxidation products. *Journal of Polymer Science Part B*. 2003;41(13):1509–1517. DOI: 10.1002/polb.10499

24 - Medeiros AS, Faria LO. Study of the long term effect of high gamma doses in the crystalline phase of P(VdF-TrFE) copolymers. *Nuclear Instruments and Methods in Physics Research Section B*. 2010;268(17):2740-2743.

25 - Medeiros AS, Faria LO. High gamma dose response of poly(vinylidene fluoride) copolymers. *Nuclear Instruments and Methods in Physics Research Section A*. 2008;587(2): 315-318.